Matthew Ernst
Applied Physics Laboratory,
Johns Hopkins University,
Laurel, MD 20723
e-mail: ernstm@gmail.com

Ed Habtour
Vehicle Technology Directorate,
U. S. Army Research Laboratory,
Aberdeen Proving Ground, MD 21005
e-mail: ed.m.habtour.civ@mail.mil

Abhijit Dasgupta
Center for Advanced Life Cycle Engineering,
University of Maryland,
College Park, MD 20742
e-mail: dasgupta@umd.edu

Michael Pohland
U.S. Army Materiel System Activity Analysis,
Aberdeen Proving Ground, MD 21005
e-mail: michael.f.pohland.civ@mail.mil

Mark Robeson
U.S. Army's Aviation Development
Directorate at Ft. Eustis,
Ft. Eustis, VA 23604
e-mail: mark.e.robeson.civ@mail.mil

Mark Paulus
Naval Undersea Warfare Center,
Keyport, WA 98345
e-mail: mark.paulus@navy.mil

Comparison of Electronic Component Durability Under Uniaxial and Multiaxial Random Vibrations

Multiaxial and uniaxial vibration experiments were conducted in order to study the differences in failure modes and fatigue life for the two types of excitation. An electrodynamic (ED) shaker capable of controlled vibration in six degrees of freedom (DOF) was employed for the experiments. The test specimen consisted of six large inductors insertion mounted on a printed wiring board (PWB). Average damage accumulation rate (DAR) in the inductor leads was measured for random excitations in-plane, out-of-plane, and both directions simultaneously. Under simultaneous multiaxial excitation, the average DAR was found to be 2.2 times greater than the sum of the in-plane and out-of-plane DARs. The conclusion was that multiple-step sequential uniaxial testing may significantly overestimate the durability of large/heavy structures with high center of mass in a multiaxial dynamic environment. Additionally, a test method utilizing uniaxial vibration along a direction other than the principal directions of the structure was examined. This method was found to have significant limitations, but showed better agreement with simultaneous multiaxial vibration experiments. [DOI: 10.1115/1.4028516]

Keywords: multiaxial, nonlinear, vibration, fatigue, simultaneous loading

1 Introduction

During their life-cycle, large/heavy electronics components serve in environments subject to vibratory loading. These loads may have a profound effect on the performance of electronics, the structural load distribution, and the overall reliability of components. Increasingly, electronics are required to performed complex tasks in harsh vibration environments that are multiaxial in nature [1]. These types of loads may lead to degradation and catastrophic failures in these platforms. The complex dynamic loads may impose significant stresses on the printed circuit board (PCB) substrate, component packages, leads, and solder joints [1,2]. In addition, the reliability of electronic systems exposed to vibration environment depends primarily on the vibration responses of the internal components over a wide frequency range. The variation in packaging configuration may present more complication to the systems such as nonlinear dynamic effects due to high amplitude vibration loads and multiaxial excitation. It is, therefore, imperative to simulate realistic "real-world" multiaxial test environment to identify vibration-induced fatigue failure modes, estimate the DARs and assess the reliability of the product. Commonly, vibration shakers are employed during product development to assess reliability and ensure product safety before products enter production or service. Until recently, test laboratories using ED shakers were restricted to single-axis-at-a-time (sequential) methods due to a lack of multiaxial test equipment. Unfortunately, sequential vibration testing often produces misleading and nonconservative predictions of time to failure (TTF) in electronics. Still today, many consider newly available multiple degree-of-freedom (MDOF) ED test equipment too expensive for practical applications. As a result, test strategies utilizing only uniaxial vibration shakers are still the mainstay of product development testing. Unfortunately, the literature does not provide any methodology that considers multiaxial vibration in electronics systems [3]. Several researchers studied high-cycle fatigue in circuit card assemblies (CCAs) exposed single-axis harmonic and random excitations in the range of 10 Hz to 10 kHz [3]. Based on an extensive literature review conducted by Habtour et al. [3], multiaxial vibration studies in electronics components are limited. This paper examines how well two uniaxial test methods approximate the damage incurred under true multiaxial vibration using a novel simultaneous multiaxial base excitation ED shaker. Nonlinearities due to high amplitude vibratory environment and multiaxial excitation are discussed, which is an area not fully understood in the electronics packaging world.

2 Experimental Approach

2.1 Overview. In widespread use are methods similar to ISO 16750-3 [4], which utilize a multiple-step procedure with one test performed in each of the three orthogonal planes. Commonly, profiles such as those found in standards such as MIL-STD-810G [5] are used as the basis for these tests. In this paper, the above approach is referred to as the multiple-step uniaxial method. Several studies have pointed out shortcomings of this test method including Refs. [6–10].

Contributed by the Electronic and Photonic Packaging Division of ASME for publication in the JOURNAL OF ELECTRONIC PACKAGING. Manuscript received June 26, 2014; final manuscript received August 24, 2014; published online October 15, 2014. Assoc. Editor: Satish Chaparala.

An alternate method for simulating a multiaxial response on uniaxial equipment involves fixturing the device under test at a skewed angle relative to the machine axis, so that excitation along the shaker's principal axis excites multiple response modes simultaneously. In this method, the excitation magnitude along each principal axis of the test specimen is determined by a coordinate transformation of the excitation vector from the machine principal axis system to the specimen (fixture) principal axis system components of excitation. In this method, the excitation histories along the different orthogonal axes of the test specimen are completely in phase and scalar multiples of each other. In other words, the power spectral densities (PSDs) for all axes are scalar multiples of each other. This approach can be simulated in the multiaxial shaker by ensuring 100% coherence between the excitation histories along orthogonal axes. The vector sum of the orthogonal excitations provides the orientation and magnitude of the resultant excitation. In this paper, this method will be referred to as the resultant PSD method.

2.2 Specimen Design. The specimen under test during this experiment was a printed wiring assembly comprised of a four layer FR-4 fiberglass/epoxy circuit board with six insertion-mounted inductors. Figure 1 shows a photograph of the test specimen. Figure 2 shows a dimensioned layout of the test specimen with component labels and a *XYZ* coordinate system for reference. The board thickness was approximately 1.71 mm and the component stand-off was approximately 2 mm. The inductors were mounted to the circuit card such that the two connection points were oriented along the *Y* axis. This resulted in the components being less stiff in the *X* direction than in the *Y* direction. SAC305 solder was used for the interconnects.

Details of the inductor construction are shown in Figs. 3–8. The inductors were Bornes model No. 5604-RC. The inductor's dimensions are shown in Fig. 6. Each inductor weighed approximately 23 g, and composed of 1.07 mm film insulated copper wire wound around a ferrite bobbin core. Additionally, small insulating sleeves were around the copper wire, where it exited the bobbin.

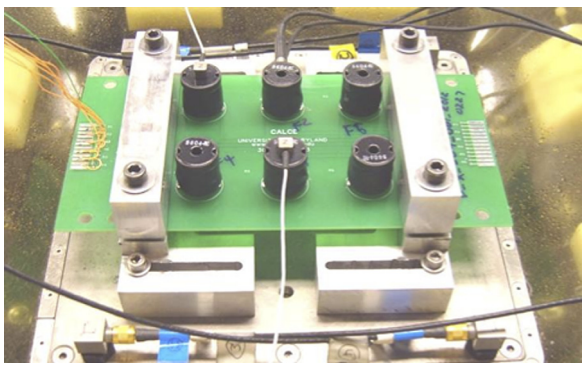

Fig. 1 Photograph of test specimen on shaker table

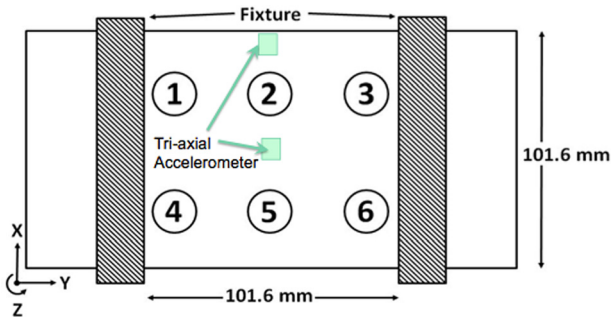

Fig. 2 Test specimen schematic

Fig. 3 External view of inductor

Fig. 4 Inductor with shrink wrap removed

Fig. 5 Inductor with tape wrap removed

Adhesive tape was wrapped around the copper windings and shrink wrap tubing covered the outside of the inductor, as shown in Figs. 4 and 5. Figures 7 and 8 show that the wire coil winding created an asymmetry in the construction, which was not immediately apparent before the physical teardown of the component.

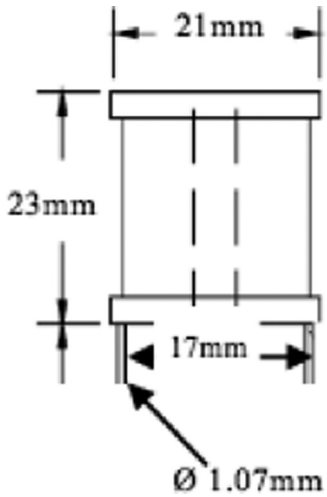

Fig. 6 Inductor dimensions

Fig. 7 Outside coil wrap (stiff lead)

Fig. 8 Inside coil wrap (compliant lead)

The lead corresponding to the outside coil wrap was held tightly in place by the shrink-wrap, while the inner coil wrap was relatively unrestrained, creating a comparatively compliant lead. As a result, 98% of the failures produced in this investigation occurred in lead corresponding to the outside wrap.

2.3 Fixturing and Instrumentation. The circuit card was rigidly clamped to the shaker table along two edges with aluminum fixture clamps, as shown in Figs. 1 and 2. The unsupported span between the clamps was 101.6 mm. A torque of 15 N m was applied to each of the four bolts holding the clamp. The inductors were electrically connected to pads on the edge of the card to allow monitoring the interconnect impedance for failure detection during the tests. Eight tri-axial accelerometers were used during the tests. Four of these tri-axial accelerometers were mounted on the table top at the four corners to monitor and control excitation. Four additional accelerometers were used to monitor specimen motion. Since the components are mounted symmetrically on the CCA, lightweight (1 g) tri-axial accelerometer was attached to the edge component (components 1) and a center component (component 5) at the top center of the components bodies, as shown in Fig. 1. The purpose of this layout is to provide an overall picture of the response of all the components. Additionally, two tri-axial accelerometers were mounted on the bottom-side center of the board and top-side rear edge of the board to capture the bending and twisting modes of the CCA.

3 Dynamic Characterization

Analysis of acceleration response data combined with finite element modeling (FEM) yielded an understanding of the vibration modes of the system [11]. The accelerometers inertial contributions were included in the analysis. The model assumes that the PCB is rigidly clamped along two edges and free along the other two, as shown in Fig. 2. The material properties used in analysis are tabulated in Table 1, which includes the Young's modulus, E, shear modulus, Poisson's ratio, and density. Vibration modes I–VI corresponded to component motion in the X direction with each component having a slightly different fundamental frequency. In this study, the component fundamental modes fundamental modes in the Y and Z directions were ignored, since they were much higher than board twist mode, which were outside the PSD profile. The measured frequency of the components fundamental modes was generally between 68 and 90 Hz, with the exact frequency depending on several factors including component location on the card (boundary condition effect), differences in mass due to the presence of accelerometers, manufacturing variability of each component, variation in stand-off height during assembly and damage accumulation in the leads. A representative depiction of one of these modes is shown in Fig. 9, showing the modal displacement magnitude. As expected, the fundamental modes of the components with accelerometers were approximately 2 Hz lower than the ones without the accelerometers. Modes VII and VIII of the system corresponded to (0,2) transverse bending of the board and (1,2) twisting of the board as shown in Figs. 10 and 11, respectively. The corresponding modal frequencies for modes VII and VIII were measured to be approximately 176 Hz and 214 Hz, respectively. The next higher mode of the system is a (0,3) mode. The response frequency for this mode was seen through FEM to be approximately 387 Hz. As this was above the maximum cut-off frequency of the input excitation PSD, no excitation of this mode or higher order modes was observed.

In this study, a unique and novel six degree-of-freedom multiaxial ED shaker was utilized to impose uniaxial and multiaxial base excitations. As shown in Fig. 12, the shaker consists of twelve ED actuators mechanically coupled to a 20.32 cm $\times$ 30.32 cm (8 in. $\times$ 8 in.) table. Eight actuators are located in plane while four of the actuators are out-of-plane and located underneath the shaker table. The shaker architecture allows the system to produce a highly controlled multiaxial vibration environment with independent control over 6DOF: three translations and three rotations. However, in this study, only translational motion in two of the axes (X: in-plane and Z: out-of-plane) was excited, to investigate the effect of multiaxial base excitations on large/heavy electronic components. Further information on this 6DOF shaker table is available in Refs. [1,12]. Control, data

Table 1 Materials properties

Part	Material	E_X (MPa)	E_Y (MPa)	G_{ZX} (MPa)	Poisson's ratio	Density (g/cm^3)
Leads	C197	1F.4	118.4	—	0.3	8.84
PWB	FR4	18.6	18.6	0.13	—	1.85
Inductor	Rigid mass	N/A	N/A	N/A	N/A	N/A
Accelerometer	Rigid mass	N/A	N/A	N/A	N/A	N/A

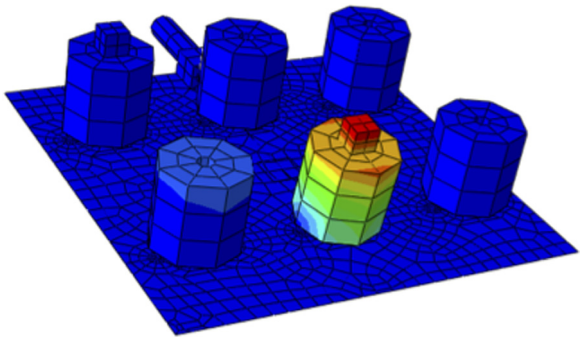

Fig. 9 Vibration mode I

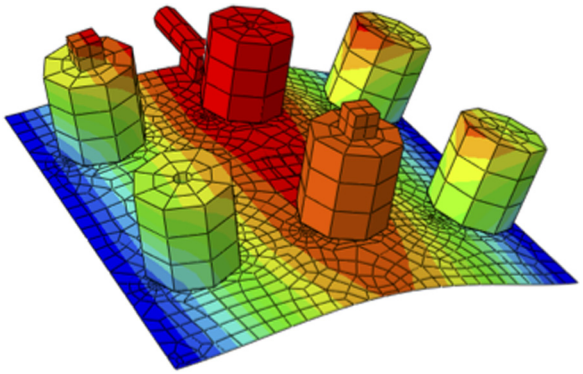

Fig. 10 Vibration mode VII

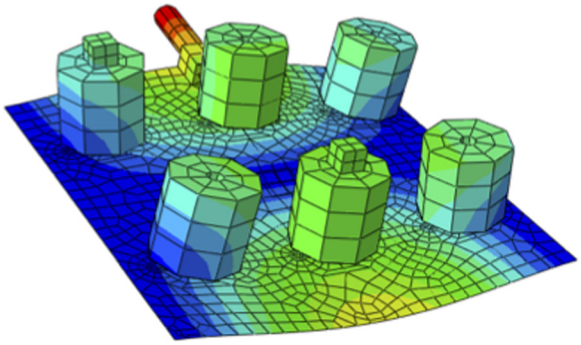

Fig. 11 Vibration mode VIII

acquisition, and in-test monitoring were accomplished using a special MDOF data acquisition unit and custom software.

4 Experimental Setup

Failure was defined as a break in continuity of the electrical connection between the circuit card and component body. The circuit cards were tested until all six original components failed. When a component failed, the test was paused and the failed component was desoldered and removed from the card. To preserve the dynamics of the test card, a new identical dummy component was resoldered in its place. With the failed component replaced, the vibration test was resumed and continued until another component failed. This process was repeated until all six original components failed. Durability (TTF) for each component was recorded as the total time the shaker was at full operating level until loss of electrical continuity of that component. Downtime during component replacement was not included in the durability estimation.

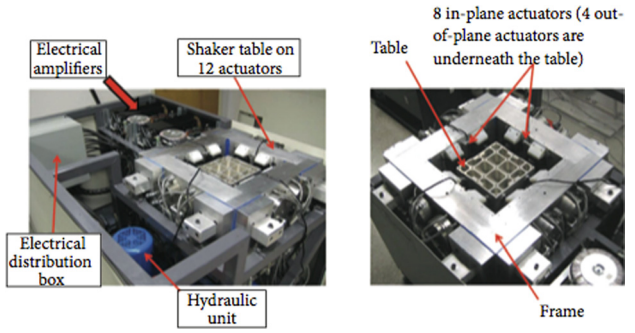

Fig.12 MDOF shaker (partially disassembled)

The random vibration excitation levels used for the durability test were based on the electronics screening profile recommended in the U.S. Navy's manufacturing screening program document NAVMAT P9492 [13]. The profile's frequency range was modified to better accommodate the test specimen and project objectives. The original NAVMAT profile calls for vibration up to 2000 Hz. In order to reduce the complexity of the test article's response, the excitation profile in this study (labeled "CALCE profile") was truncated at 320 Hz, with a roll-off starting at 250 Hz. The purpose was to limit the response to as few PWB modes as possible. For the excitation profile shown above, the response included the first eight modes (six component deflection modes and two PWB deflection modes, shown earlier in Figs. 9–11). The first two PWB modal frequencies were too close to allow selective excitation of either mode, and were hence both included. The PSD function for the NAVMAT P9492 profile and for this durability test profile (labeled "CALCE profile") can be seen in Fig. 13. The total G_{rms} from 20 Hz to 320 Hz for the CALCE profile was 3.14.

Four experiments were conducted in order to evaluate the performance of the two uniaxial test methods discussed above, in comparison to a true multiaxial test. The experiments are summarized in Table 2. Experiments 1 and 2 were used to establish average DARs for in-plane and out-of-plane excitations, respectively. Experiment 3, on the other hand, utilizes two axes of the shaker at near zero coherence between the two specified axes. One of the two axes is in the plane of the PWB and the other is in the out-of-plane direction. This is considered a true multiaxial vibration environment. Experiment 4 is representative of the resultant PSD method. By specifying the same vibration profile for each axis with a near 100% coherence between the two axes, the effect was to create vibration input along the resultant axis (45 deg off the out-of-plane direction in this case) at the resultant magnitude $\sqrt{2}$ times the profile given in Fig. 13 in this case. This would be equivalent to fixturing the specimen to the table at a 45 deg angle.

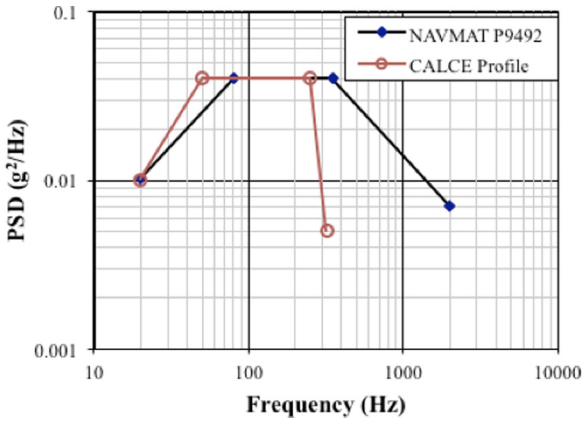

Fig. 13 Vibration power spectral density functions

Table 2 Random vibration test conditions matrix

Number	Axis	Cross-axis coherence
1	In-plane only (*X* direction)	N/A
2	Out-of-plane only (*Z* direction)	N/A
3	Combined (*X* and *Z* directions)	0.1 (incoherent)
4	Combined (*X* and *Z* directions)	0.9 (coherent)

Table 3 Component total TTF

	Component total TTF (h:min)						
Test conditions	1	2	3	4	5	6	Average
In-plane	7:55	4:52	7:25	5:47	5:06	4:17	5:54
Out-of-plane	2:32	7:25	6:42	6:21	2:55	8:01	5:39
Combined incoherent	1:11	0:42	0:45	1:40	2:01	1:41	1:21
Combined coherent	1:04	0:52	1:07	0:48	0:51	0:45	0:55

5 Results

5.1 Durability Results: Uniaxial Versus Multiaxial MDOF Excitation. The total TTF for each component during the four tests is presented in Table 3. An average DAR is defined as the reciprocal of the total TTF with units of s^{-1}. Average DAR from the total TTF data is presented in Fig. 14. Average failure time and standard deviations are calculated for the six components on each test specimen. In addition to the average DAR for each single-axis test and the low coherence combined test, a calculated hypothetical DAR for the linear superposition of in-plane and out-of-plane vibration is included in Fig. 14. These values were calculated using the linear superposition principle by summing the in-plane and out-of-plane DARs (labeled as "superposition" in Fig. 14) [14]. This linear superposition DAR represents the hypothetical total DAR expected if there are no interactions between the two axes when both axes are simultaneously excited. The computed superposition DAR was directly compared to the true "combined" DAR which was actually measured in this study under simultaneous MDOF excitation (Test 3 described above). This comparison allows us to understand the nonlinear interactions (if any) between the orthogonal excitation axes used for the simultaneous MDOF test. The results shown in Fig. 14 indicate that linear superposition methods based on sequential uniaxial testing may drastically under-represent the true DARs achieved under simultaneous multiaxial excitation. For this test specimen, a sequential uniaxial test would overestimate product durability by more than a factor of 2. This quantitative conclusion is specific to the test specimen examined in this study and should not be used as a general correction factor for other structures. The magnitude of the durability difference between sequential uniaxial tests and simultaneous MDOF tests depends on the amount of nonlinear cross-axis interactions. The specimen represents a severe case of such interactions for two reasons. First, each direction of loading excites different modes but each of these modes creates large stresses at the same location (the component lead). Second, the high mass and high radius of gyration of the inductor components creates nonlinear geometric and rotary inertia effects that cause cross-axis interactions under simultaneous in-plane and out-of-plane vibration excitation. This issue is discussed further in Ref. [15]. Even though this specimen architecture represents an extreme case, the

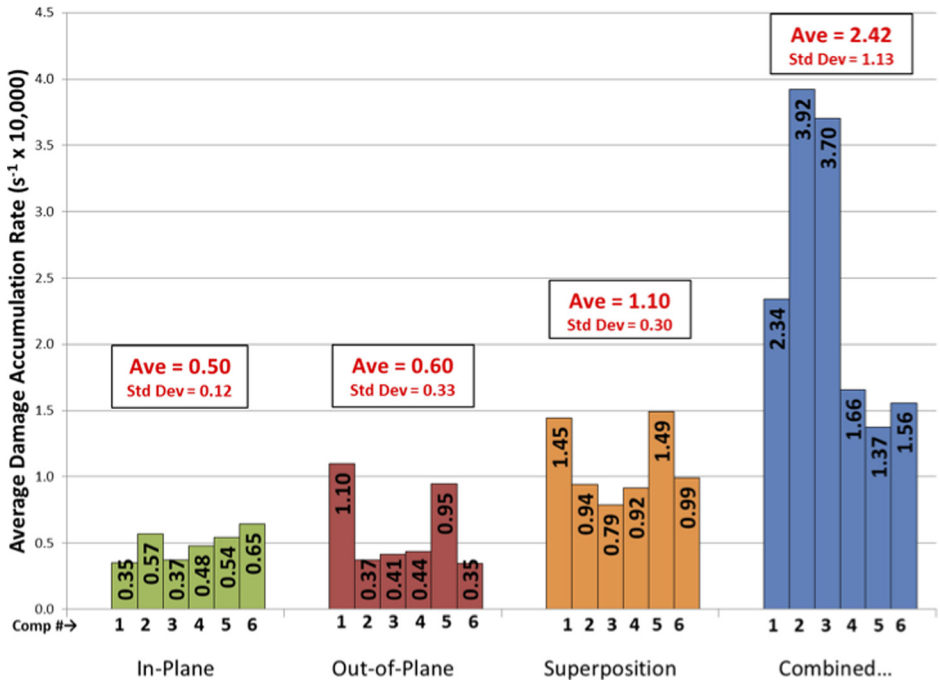

Fig. 14 Single-axis and combined-axes (incoherent) average DARs

results can be used to gain some understanding of how nonconservative sequential uniaxial test methods can be. Further studies are essential to develop meaningful correction factors for sequential uniaxial vibration testing for a broad range of structures.

5.2 Nonlinear Dynamic Response. As mentioned above, there were significant deviations between the linear superposition method and the combined excitation results. This is because the system became nonlinear under simultaneous multiaxial excitation. The dynamic nonlinearity can be clearly noticed in the acceleration response (in the x direction) measured on top of component L5, under uniaxial and multiaxial excitations, shown in Fig. 15. This response undoubtedly shows that the flexural movement of the component on the PWB, under simultaneous multiaxial excitation along the x (in-plane) and z (out-of-plane) directions is much higher than the linear sum of the individual responses under uniaxial excitations separately in the x and z directions. This amplification is symptomatic of structural dynamic nonlinearity [3]. This synergistic magnification under multiaxial excitation due to nonlinear cross-axis interaction is responsible for an amplification in the fatigue DAR under simultaneous multiaxial excitation, as discussed in Sec. 5.1.

Low and high amplitude PSD excitations were conducted to investigate the deviations between the linear superposition method and the combined excitation and confirm the present of nonlinearity. In the first, low amplitude PSD excitation of 0.0025 g^2/Hz and 0.78 G_{rms} was applied. As shown in Fig. 16, the linear superposition slightly underestimates the component response. The deviation between the linear superposition and combined excitation increases as the PSD excitation level is increased to 0.04 g^2/Hz and 0.78 G_{rms}, shown in Fig. 17. This is a clear indication that the system is nonlinear [16].

The cross-axis interaction can activate three types of nonlinear effects. First, each direction of loading produces separate modal response with high amplitudes, energies of the different nonlinear modes of vibrations can be pumped over from one mode to another [17,18]. Second, the high radius of gyration of the inductor components creates a geometric nonlinearity under cross-axis vibration, which is proportional to: (1) the velocities consistent with viscous damping forces (nonlinear rotary inertia) and (2) the displacement consistent with the restoring forces (nonlinear geometric stiffness). Finally, the components' heavy mass and high center of mass produce inertial nonlinearities as the excitation amplitude is increased. This nonlinearity causes a softening effect and a drop in the component's fundamental frequency, as shown in Fig. 15.

It is important to point out that the CCA amplification of the flexural response of the component is dominated by the nonlinear rotary inertia of the component and it is instructive to consider the underlying nonlinear dynamics of this structure. For simplicity, consider the component idealized as a beam with a large tip mass. It is well known in the literature [17–19] that when such a beam is

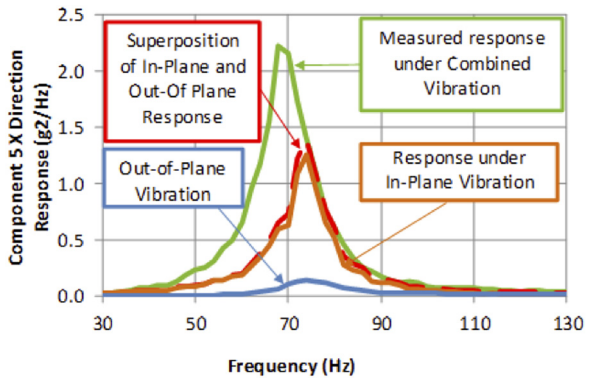

Fig. 15 Multiaxial response amplification for component flexure in the *x* direction

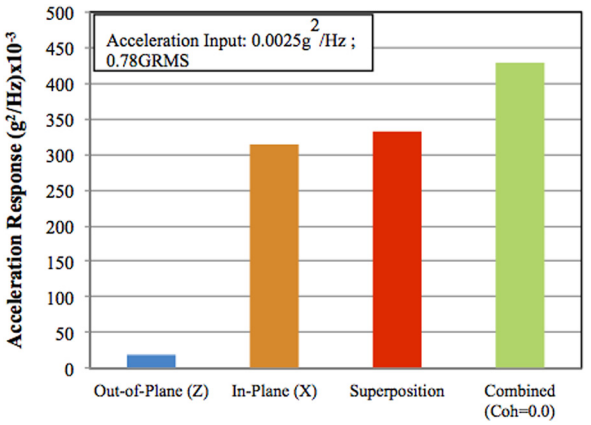

Fig. 16 Comparison between combined multiaxial excitation and superposition at 0.78 G_{rms}

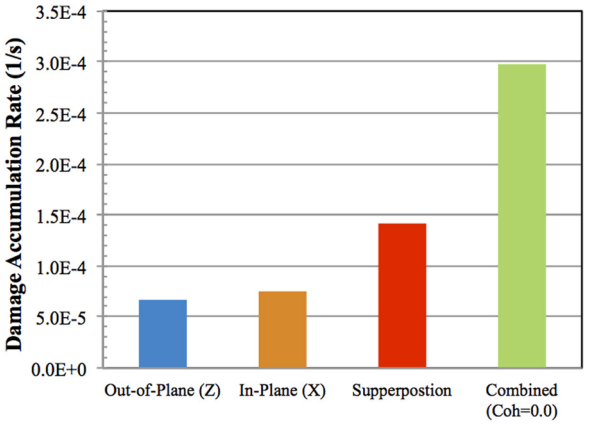

Fig. 17 Comparison between combined multiaxial excitation and superposition at 3.14 G_{rms}

subjected to high amplitude harmonic translational excitation simultaneously along the axial and transverse directions, the flexural response experiences a nonlinear amplification if the axial excitation is at twice the frequency of the transverse excitation and the phases of the two excitations are integer multiples of each other. Figures 16 and 17 show that, indeed, for the test vehicle used in this study, the modal response of the circuit card (at approx. 170–180 Hz) transmits (pumped) axial excitation to the base of the component at approximately twice the transverse (flexural) natural frequency of the component (at approx. 80–85 Hz); see Fig. 18. Thus, the condition for nonlinear cross-axis amplification is indeed satisfied in this structure, and hence the response amplification is significantly large under simultaneous multiaxial excitation, as was seen earlier in Figs. 16 and 17. The effect of this response amplification due to the dynamic nonlinearities instigated by multiaxial excitation magnifies the fatigue DAR, making the superposition method unsuitable. It is important to point out that the nonlinear beam example is selected as a simplified idealistic representation to illustrate the underlying nonlinear response of the component, but does not address all the complexities associated with the CCA, such as material nonlinearities, the PWB nonlinear response (nonlinear plate), nonlinear boundary conditions of the CCA, nonlinear interaction between the plate and the components (including the nonlinear behavior of the soldered interconnection), or dynamic interactions between the components.

5.3 Durability Results: Resultant PSD Method Versus Multiaxial Excitation. Average DARs for the incoherent (Test 3) and coherent (Test 4) multiaxial ("combined") tests are presented

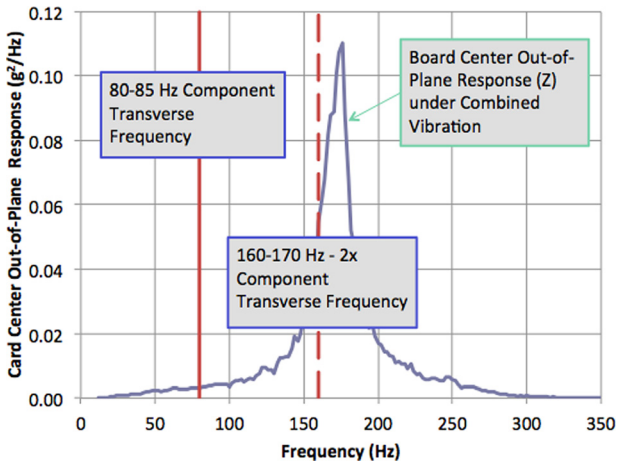

Fig. 18 Measured PWB response in out-of-plane, *z* direction

in Fig. 19. As discussed earlier, Test 4 provides resultant uniaxial excitation along a skewed direction represented by the vector sum of the orthogonal excitations along the different shaker axes. The durability results suggest that although the resultant PSD test method cannot fully mimic a true multiaxial test, it is not as inaccurate as sequential uniaxial testing, for assessing vibration durability in true simultaneous multiaxial environments. While, at first look, this method may seem like a promising method to avoid the use of complex MDOF test equipment, one must keep in mind

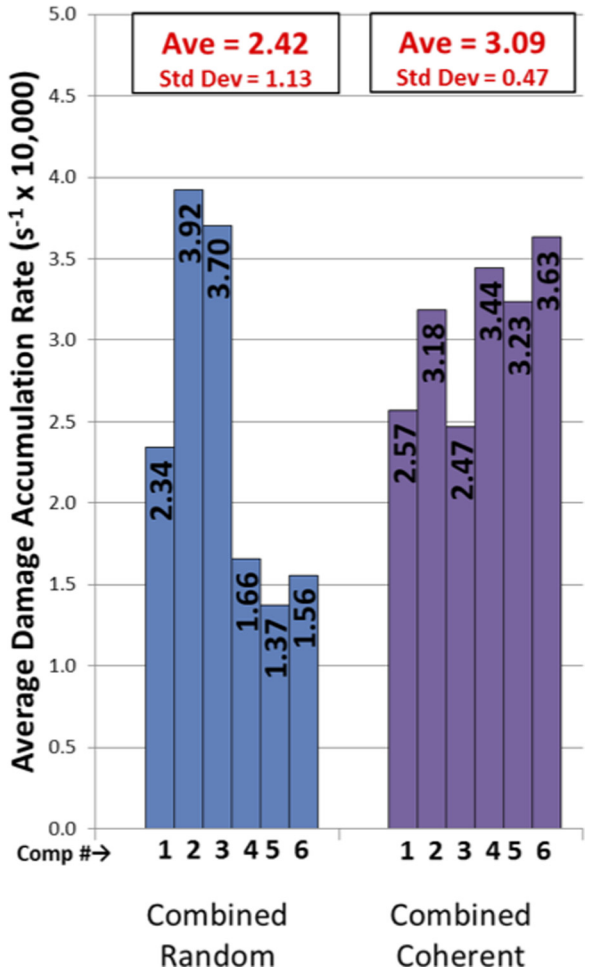

Fig. 19 Coherent and incoherent average DARs

that this method can only work when the vibration PSD profiles on orthogonal axis, are scalar multiples of each other (in other words there is 100% coherence between the orthogonal axes). True vibration environments generally do not satisfy this simplifying constraint. Furthermore, the limited number of vibration modes and independence of the modes in the test structure used in this study may have further favored this test method. The results may not be as favorable for more complex structures and more complex environments. Further studies are recommended to understand how the resultant PSD method performs for different types of test structures.

6 Conclusion

The experimental study reveals the importance of understanding the nonlinear dynamic characteristics of devices in order to correlate the defects with the dynamic responses under multiaxial loading. This study overcomes the intrinsic disadvantages of most of the existing theoretical and experimental studies, where the focus has traditionally been on sequential uniaxial excitation combined with superposition of the response to each axis. However, linear superposition is incapable of capturing nonlinear behaviors. The superposition approach is inaccurate when the amplitudes of oscillations are sufficiently high for multiaxial excitation. Therefore, the nonlinear dynamic characteristics of CCAs under multiaxial excitation must not be ignored. The results presented in this study can be exploited to gain an understanding of how to avoid misrepresentative sequential uniaxial test methods. Further studies are essential to develop meaningful correction factors for multistep uniaxial vibration testing, for a broad range of structures.

7 Future Efforts

Potential future work includes application to Army vehicles, including those with known characteristics of driving frequencies, such as rotorcraft. The opportunity for better understanding the interaction of those driving frequencies can lead to more efficient and effective design processes, as well as more durable designs. Also, the opportunity for increased efficiency of test and/or analysis of structural modifications, component installations, or mission equipment installations offers a better path forward for avoiding destructive resonance and extending vehicle/component life. CALCE is working jointly with the U.S. Army, national laboratories and academia to enhance current guidelines, and procedures for multiaxial vibration testing.

Acknowledgment

This research effort was funded by the sponsors of the Center for Advanced Life Cycle Engineering (CALCE) at the University of Maryland and was further supported by a Collaborative Research and Development Agreement (CRADA) between the U.S. Army Research Laboratory and the University of Maryland, College Park, MD. We gratefully acknowledge the continual support of Naval Undersea Warfare Center and for the unique MDOF test setup provided by TEAM Inc. and Data Physics Inc.

References

[1] Habtour, E., Choi, C., Drake, G., Dasgupta, D., and Al-Bassyiouni, M., 2010, "Improved Reliability Testing With Multiaxial Electrodynamics Vibration," 56th Annual Reliability and Maintainability Symposium (RAMS), San Jose, CA, Jan. 25–28.
[2] Yu, D., Al-Yafawi, A., Nguyen, T. T., Park, S., and Chung, S., 2011, "High-Cycle Fatigue Life Prediction for Pb-Free BGA Under Random Vibration Loading," Microelectron. Reliab., **51**(3), pp. 649–656.
[3] Habtour, E., Connon, W., Pohland, M. F., Stanton, S. C., Paulus, M., and Dasgupta, A., 2014, "Review of Response and Damage of Linear and Nonlinear Systems Under Multiaxial Vibration," Shock Vib. J., **2014**, p. 294271.
[4] ISO, 2003, "Road Vehicles—Environmental Conditions and Testing for Electrical and Electronic Equipment," International Organization for Standardization, Geneva, Switzerland, Standard No. ISO 16750.

[5] Department of Defense, 2008, "Enviromental Engineering Considerations and Laboratory Tests," U.S. Department of Defense, Washington, DC, Test Method Standard MIL-STD 810G.
[6] Whiteman, W., and Berman, M. B., 2002, "Fatigue Failure Results for Multiaxial Versus Uniaxial Stress Screen Vibration Testing," J. Shock Vib., **9**(6), pp. 319–328.
[7] Himelblau, H., Hine, M., Frydman, A., and Barrett, P., 1995, "Effects of Triaxial and Uniaxial Random Excitation on the Vibration Response and Fatigue Damage of Typical Spacecraft Hardware," 66th Shock and Vibration Symposium, Biloxi, MS, Oct. 30-Nov. 3.
[8] French, R., Handy, R., and Cooper, H. L., 2006, "A Comparison of Simultaneous and Sequential Single-Axis Durability Testing," Exp. Tech., **30**(5), pp. 32–37.
[9] Gregory, D., Bitsie, F., and Smallwood, D., 2008, "Comparison of the Response of a Simple Structure to Single Axis and Multiple Axis Random Vibration Inputs," 79th Shock and Vibration Symposium, Orlando, FL, Oct. 26–30.
[10] Paulus, M., Dasgupta, A., and Habtour, E., 2012, "Life Estimation Model of a Cantilevered Beam Subjected to Complex Random Vibration," Fatigue Fract. Eng. Mater. Struct., **35**(11), pp. 1058–1070.
[11] Yu, D., Al-Yafawi, A., Park, S., and Chung, S., 2010, "Finite Element Based Fatigue Life Prediction for Electronic Components Under Random Vibration Loading," 60th Electronic Components and Technology Conference (ECTC), Las Vegas, NV, June 1–4, pp. 188–193.
[12] Habtour, E., Choi, C., Osterman, M., and Dasgupta, A., 2012, "Novel Approach to Improve Electronics Reliability in the Next Generation of U.S. Army Small Unmanned Ground Vehicles Under Complex Vibration Conditions," J. Failure Anal. Prev., **12**(1), pp. 86–95.
[13] U.S. Navy, 1979, "Navy Manufacturing Screening Program," U.S. Department of the Navy, Naval Material Command, Standard No. NAVMAT P-9492, pp. 9–14.
[14] Wirsching, P. H., Paez, T. L., and Ortiz, K., 1995, *Random Vibrations: Theory and Practice*, Wiley, New York.
[15] Ernst, M., 2013, "Response and Durability of Large Radius of Gyration Structures Subjected to Biaxial Vibration," M.S. thesis, Department of Mechanical Engineering, University of Maryland, College Park, MD.
[16] Worden, K., and Tomlinson, G. R., 2001, *Nonlinearity in Structural Dynamics: Detection, Identification, and Modelling*, Institute of Physics, Bristol, UK.
[17] Balachandran, B., and Nayfeh, A. H., 1991, "Observations of Modal Interactions in Resonantly Forced Beam-Mass Structures," Nonlinear Dyn., **2**(2), pp. 77–117.
[18] Malatkar, P., and Nayfeh, A. H., 2003, "A Parametric Identification Technique for Single-Degree-of-Freedom Weakly Nonlinear Systems With Cubic Nonlinearities," J. Vib. Control, **9**(3–4), pp. 317–336.
[19] Kumar, V., Miller, K. J., and Rhoads, J. F., 2011, "Nonlinear Parametric Amplification and Attenuation in a Base-Excited Cantilever Beam," J. Sound Vib., **330**(22), pp. 5401–5409.